

## 4.3 GNC and ADCS

*Sub-Section Authors: An-Ya Olson and Matthew Coleman*

### 4.3.1 Key Requirements

*The GNC subsystem shall...*

- Sense the position of the spacecraft center of mass relative to the Sun.
- Stabilize the spacecraft during impulsive burns and be able to correct for the worst case misalignment of the thrust vector from the center of mass.
- Perform momentum unloading to rid the spacecraft of any disturbance torques that accumulate.
- Perform stationkeeping to maintain the desired orbits around L3, L4, and L5.

*The ADCS subsystem shall...*

- Sense the attitude of the body axes of the spacecraft relative to the Sun.
- Provide full 360° slew capabilities to enable transfer from launch vehicle to on-station operation.
- Maintain a pointing accuracy of 10° to the Sun during the transfer ellipse to L3, L4, and L5.
- Maintain a pointing accuracy of 0.2° to the Sun center of mass within 95% confidence during imaging (driven by LASCO, the coronagraph replacing CCOR)

### 4.3.2 ADCS Operations During Control Modes

*Table 4.3-1: Summary of ADCS Operations During Control Modes*

Mode	Description	ADCS Operations
<i>Transfer and Acquisition</i>	Astrodynamic and attitude-control maneuvers only	Stabilize spacecraft during impulsive maneuvers, keep sun-pointing during transfer ellipse, slews to reorient for thermal needs.
<i>On-station</i>	All systems and payloads necessary to complete mission will be active	Meet full pointing-requirements.
<i>Limited Operations</i>	≈60% of “On Station”	Same as On-station
<i>Safe</i>	Minimal communication; only power requirements are those required to keep the spacecraft at the Lagrange Points	Maintain any halo orbit about the Lagrange points.

### 4.3.3 Spacecraft Body Axes Configuration

Figure 4.3-1 shows the configuration of body frame axes used for all of the subsequent analyses and simulations. The directions of the three axes are consistent with the directions decided by the structures team (see Section 6.2.3.3) for all of the structural analyses in CREO. During on-station operations, the  $\hat{b}_x$  axis is meant to point towards the Sun at all times. Note that the origin of the three axes, denoted by the green dot, lies at the center of mass of the spacecraft which shifts throughout the mission lifetime based on fuel usage; its location in the diagram is arbitrary.

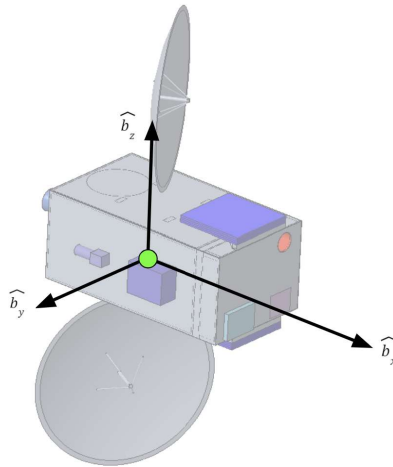


Figure 4.3-1: Spacecraft Body Axes Configuration

### 4.3.4 Analysis of GNC and ADCS Maneuvers

In order to analyze some of the key maneuvers the subsystem must be capable of handling, it was useful to simulate the satellite rotation using MATLAB, and from there to implement a control law to perform “regulation,” that is, slewing the spacecraft with an instantaneous control rotation. While this is possible by linearizing Euler’s equations of rotational motion, that method does not hold true for maneuvers with varying angular velocity, and in general, treating the system as linear time-invariant (LTI) makes some simplifications in this case which can degrade the quality of the results. A more rigorous analysis, the one which will be performed here, involves the use of quaternions to parameterize the rotation of the spacecraft and a PD controller to apply the control torque.

In this section, let quaternions be defined as a 4-component vector in the form  $q = \hat{q}_1 \hat{i} + \hat{q}_2 \hat{j} + \hat{q}_3 \hat{k} + q_4$ , such that  $\hat{i}^2 = \hat{j}^2 = \hat{k}^2 = \hat{i}\hat{j}\hat{k} = -1$ . These rules naturally yield two definitions for multiplication, one of which is denoted by  $\otimes$  for attitude control purposes:

$$\bar{\mathbf{q}} \otimes \mathbf{q} = \begin{bmatrix} q_4 \bar{\mathbf{q}}_{1:3} + \bar{q}_4 \mathbf{q}_{1:3} - \bar{\mathbf{q}}_{1:3} \times \mathbf{q}_{1:3} \\ \bar{q}_4 q_4 - \bar{\mathbf{q}}_{1:3} \cdot \mathbf{q}_{1:3} \end{bmatrix}$$

Equation 4.3-1

where  $q_{1:3}$  denotes the imaginary components of  $q$ , and  $q_4$  denotes the scalar. The control law used is as follows:<sup>70</sup>

$$\delta \mathbf{q} = \begin{bmatrix} \delta \mathbf{q}_{1:3} \\ \delta q_4 \end{bmatrix} = \mathbf{q} \otimes \mathbf{q}_c^{-1}$$

$$\mathbf{L} = -k_p \operatorname{sign}(\delta q_4) \delta \mathbf{q}_{1:3} - k_d \boldsymbol{\omega}$$

Equation 4.3-2

where  $\bar{L}$  is the control torque and  $\delta q$  is the “error” quaternion, defined as the cross product between the current rotation quaternion  $q$  (between an inertial frame and the satellite body frame) and the inverse of the commanded quaternion  $q_c$ . In this way,  $\delta q = I_q = 1$ , the identity quaternion, when  $q$  and  $q_c$  are superimposed, or in other words, the command input is satisfied. Euler’s equations of rotational motion are then integrated along with this control torque:

$$\begin{aligned} \dot{I}\boldsymbol{\omega} &= -[\boldsymbol{\omega} \times]I\boldsymbol{\omega} + \bar{L} \\ \dot{h} &= -[\boldsymbol{\omega} \times]h - \bar{L} \end{aligned}$$

Equation 4.3-3

where,  $I$  represents the inertia matrix,  $h$  is the angular momentum, and  $\dot{h}$  is the rate of change of angular momentum. Integrating the control torque through any of the satellite maneuvers allows one to determine the equivalent control angular momentum rate of change ( $\dot{h}$ ) which would need to be applied in the body frame, as well as the control angular momentum ( $h$ ) for each time step, and from there it is straightforward to decompose this vector into each of four wheels in two different configurations, a pyramidal configuration and the NASA standard configuration:<sup>71</sup>

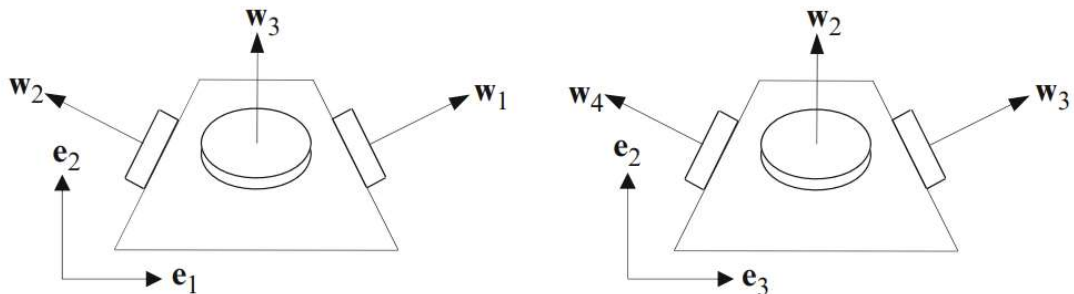


Figure 4.3-2a: Pyramid reaction wheel configuration

<sup>70</sup> Markley, F. Landis. (2014). *Fundamentals of Spacecraft Attitude Determination and Control*. Springer.

<sup>71</sup> Markley, F. Landis. (2014). *Fundamentals of Spacecraft Attitude Determination and Control*. Springer.

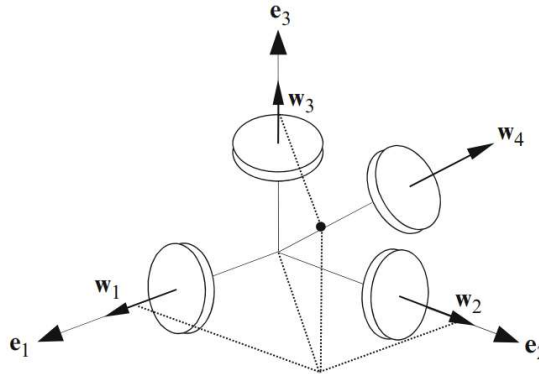


Figure 4.3-2b: NASA reaction wheel configuration<sup>72</sup>

This is done by multiplying the angular momentum vector  $h$  by the Moore-Penrose pseudoinverses of the following distribution matrices which account for the geometries of the pyramid and NASA configurations, respectively:

$$\mathcal{W}_4 = \frac{1}{\sqrt{2}} \begin{bmatrix} 1 & -1 & 0 & 0 \\ 1 & 1 & 1 & 1 \\ 0 & 0 & 1 & -1 \end{bmatrix}, \quad \mathcal{W}_N = \begin{bmatrix} 1 & 0 & 0 & 1/\sqrt{3} \\ 0 & 1 & 0 & 1/\sqrt{3} \\ 0 & 0 & 1 & 1/\sqrt{3} \end{bmatrix}$$

Equation 4.3-4

The inertia tensor used in these simulations is the inertia tensor for the L3 satellite (the heaviest of the 3), which is the “worst case” configuration for ADCS, since any slew maneuver will be the most costly fuel-wise due to the L3 satellite’s higher mass. Additionally, since the controller will “unknowingly” exert impossible amounts of torque to perform a maneuver, the gains  $k_p$  and  $k_d$  are tuned individually for each simulation to the point that the satellite’s actuators are physically capable of delivering the required torque and the momentum wheels will not be saturated over the duration of the mission.

All of the code and plots generated for this analysis can be found in this Github repository: [https://github.com/amolson2/aspa\\_adcs](https://github.com/amolson2/aspa_adcs).

#### 4.3.4.1 Disturbance Rejection

##### Mathematical Models:

**Magnetic Field Torque** can be represented by the following:

$$T_m = DB = D \frac{M}{R^3} \lambda$$

Equation 4.3-5

where  $D$  is the spacecraft’s residual dipole moment (usually on the order of 1-20 A-m<sup>2</sup> or Ampere-Square Meter);  $B$  is the magnetic field strength of the central body in Teslas;  $M$  is the magnetic moment of the central body multiplied by the magnetic constant;  $\lambda$  is a unitless

function of magnetic latitude ranging from 1 to 2.<sup>72</sup> A dipole moment of 20 Am<sup>2</sup> was used to calculate the worst case magnetic field torque.

*Effects from the Sun:* the heliospheric magnetic field (HMF) is the portion of the Sun's magnetic field that gets 'dragged out' by the solar wind to occupy the rest of the solar system. At Earth's orbital radius around the Sun, the HMF averages about 6 nT, but can reach up to 37 nT at maximum solar cycle.<sup>73</sup>

*Effects from the Earth:* for Earth, the spacecrafts' distance from the Earth center of mass can be approximated as 1 and 2 AU, for L4/L5 and L3, respectively. M is  $7.18 \times 10^{15}$  Tm<sup>3</sup>.

**Gravity Gradient Torque** can be represented by the following:

$$T_g = \frac{3\mu}{|R|^5} (R \times IR)$$

*Equation 4.3-6*

where  $\mu$  is the standard gravitational parameter of the central body;  $R$  is the vector from the center of mass of the relevant central body to the center of mass of the spacecraft; and  $I$  is the inertia matrix of the spacecraft. The inertia matrices were obtained from the structures team. For L3,  $R$  is approximated to be 1 AU from the Sun and 2 AU from the Earth. For L4/L5, both distances are approximated as 1 AU. Since the Sun has a larger standard gravitational parameter than the Earth, the gravity gradient torque was computed with  $\mu_{sun} = 1.327 \times 10^{20}$  m<sup>3</sup>s<sup>2</sup>. The computation with cross products was performed in MATLAB.

**Solar Radiation Pressure** can be represented by the following:

$$T_s = \frac{\Phi}{c} A_s (1 + p) (r_{cp} - r_{COM}) \cos(\varphi)$$

*Equation 4.3-7*

where  $\Phi$  is the solar constant adjusted for actual distance from the Sun (1366 W/m<sup>2</sup> is the average value at 1 AU);  $c$  is the speed of light;  $A_s$  is the sunlit surface area;  $p$  is the unitless reflectance factor (ranging from 0 for perfect absorption to 1 for perfect reflection);  $r_{cp}$  is the center of solar radiation pressure;  $r_{COM}$  is the center of mass; and  $\varphi$  is the angle of incidence of the Sun.

The sunlit area of the spacecraft is approximated as 2.096 m<sup>2</sup> for the sunlit portion of the spacecraft bus, plus the solar panel area, 11.98 m<sup>2</sup> for the L3 satellite and 3.87 m<sup>2</sup> for the L4 and L5 satellites. To determine the worst case scenario for the buildup of SRP, the angle of incidence,  $\varphi$ , is assumed to be 0 and  $p$  is assumed to be 1. The solar pressure is assumed to be evenly distributed across the sun-pointing face so the center of pressure is assumed to be at the

<sup>72</sup> Larson, Wiley J., and James Richard Wertz. *Space Mission Analysis and Design*. Torrance, Calif: Microcosm, 1992.

<sup>73</sup> "Interplanetary Magnetic Field." Wikipedia. Wikimedia Foundation, October 17, 2021. [https://en.wikipedia.org/wiki/Interplanetary\\_magnetic\\_field](https://en.wikipedia.org/wiki/Interplanetary_magnetic_field).

geometric center of the spacecraft, since the spacecraft is always sun-pointing with an incident sunlight angle of  $0^\circ$ . The offset from the center of pressure from the center of mass is then calculated as the distance between the geometric center and the center of mass coordinate in the  $b_z$  direction. This is based on the on-orbit configuration determined by the structures team shown in Figure 6.2-5. These offsets were 0.0514 m and 0.0541 m for L3 and L4/L5, respectively.

**Hall Effect Thruster ‘Swirl Torque’** is brought about by the radial magnetic field component in the exit of the discharge channel of a Hall Effect thruster. This creates a velocity component on the accelerated ions and in turn imparts a reaction torque on the spacecraft. Swirl torque can be mitigated either by placing two Hall Effect thrusters next to each other such that their magnetic field components cancel out, or by treating the torque as a disturbance torque and counteracting with reaction wheels. Swirl torque is proportional to the thrust of the Hall Effect thruster; for the SMART-1 mission equipped with 70 mN Hall Effect thrusters, the swirl torque was estimated to be about  $58 \mu\text{N}$  on average during on-phases.<sup>74</sup> Given that the Hall Effect thrusters selected for all three satellites have a nominal thruster of 13 mN, this number is an appropriate worst-case estimate for the magnitude of swirl torque on the spacecraft.

*Table 4.3-2: Summary of the Disturbance Environment*

Source	Torque (Nm) for L3	Torque (Nm) for L4/L5
Magnetic Field Torque	$3.7 \times 10^{-8}$	$3.7 \times 10^{-8}$
Gravity Gradient Torque	$3.907 \times 10^{-8}$	$5.436 \times 10^{-9}$
Solar Radiation Pressure	$6.588 \times 10^{-6}$	$2.939 \times 10^{-6}$
Hall Thruster ‘Swirl Torque’	$5.8 \times 10^{-8}$	$5.8 \times 10^{-8}$
<b>Total Torque</b>	$6.722 \times 10^{-6}$	$3.089 \times 10^{-6}$

The results of this analysis verify that magnetic field torque, gravity gradient torque, and swirl torque are indeed of negligible order of magnitude compared to solar radiation pressure torque. However, in the interest of having the highest fidelity model possible, all torques are used to simulate the momentum accumulation on the spacecraft in the MATLAB model.

---

<sup>74</sup> Tremolizzo, Elena et. al., (2004). *In Flight Disturbance Evaluation of the SMART-1 Plasma Thruster*; European Space Agency, <https://adsabs.harvard.edu/full/2004ESASP.548..303T#:~:text=3.3%20Swirl%20torque%20origin%20The,C%20around%20the%20thrust%20line>.

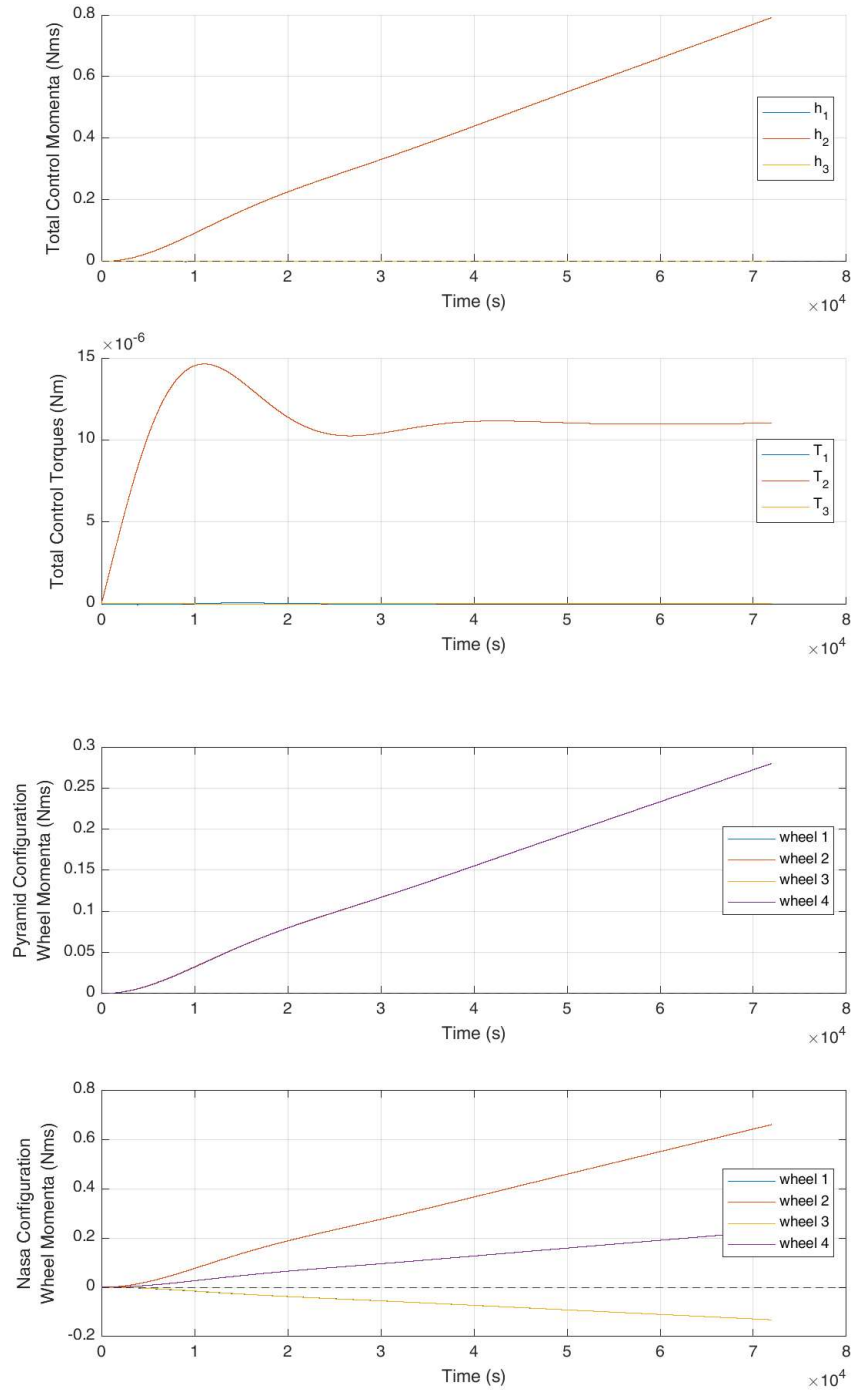


Figure 4.3-3: Environmental Disturbance Rejection Simulation (Control Momenta and Torque, And Control Momenta for Pyramid and NASA configurations)  $k_p = 5$ ,  $k_d = 10000$

For the purposes of this discussion, the worst case disturbance torque of  $6.722 \times 10^{-6}$  Nm at L3 will be used in the simulation. Through simulation, it is possible to determine how this momentum is likely to build up in each reaction wheel depending on the configuration, and from there determine how often momentum dumping must take place. The results of this simulation

are shown in Figure 4.3-3. This is done by setting  $q_c = I_q$ , or in other words, commanding the satellite to “stay put,” all the while enforcing the constant environmental torque.

These results show a constantly increasing momentum building up in the wheels at a rate of  $2.426 \times 10^{-6} \frac{\text{Nms}}{\text{s}}$  at most for the pyramid wheel configuration and  $5.718 \times 10^{-6} \frac{\text{Nms}}{\text{s}}$  for the NASA configuration. The maximum momentum increase rate in the wheels is much less than the magnitude of the environmental disturbance torque because this torque is distributed over the four reaction wheels. Given these numbers, along with the fact that the momentum capacity for each wheel is 75 Nms, the pyramid wheel configuration will saturate completely from environmental disturbance torques in approximately 357 days, and the NASA configuration will saturate in approximately 151 days. Assuming the pyramid configuration, this incurs a net momentum cost of  $1.147 \times 10^3$  Nms over the whole mission lifetime.

#### 4.3.4.2 Correcting for Main Thruster Misalignment

The potential misalignment of the main thruster during the 90 minute burn (worst case for L3 and L4) to inject into the transfer ellipse is the largest source of torque on the spacecraft to be accounted for throughout the whole mission. The misalignment torque can be calculated with the following equation:

$$T = NFL \sin(\theta)$$

Equation 4.3-8

where N is the number of thrusters, F is the nominal thruster force and  $l \sin(\theta)$  is the moment arm. The main thruster has a nominal torque of 425 N (refer to Section 6.1.2.1). The thruster nozzle will be pointed directly through the vector connecting the pre- and post-burn centers of mass so that there is never any *known* physical offset between the thrust and center of mass vectors. The angle offsets between the wet and dry centers of mass are  $3.329^\circ$ ,  $1.6423^\circ$ , and  $1.5154^\circ$  for L3, L4, and L5, respectively; these will be the degrees to which the thruster is offset from the  $b_x$  axis for each spacecraft (see Figure 4.3-1). Therefore the only source of misalignment is the potential  $0.1\text{--}0.5^\circ$  uncertainty in the precision of the thruster nozzle angle and the exact direction of the exhaust plume.<sup>75</sup> For the purposes of this analysis, a misalignment angle of  $0.2^\circ$  is assumed. This was based on further research which found that the misalignment angle is normally closer to  $0.2^\circ$ .<sup>76</sup> When the misalignment angle is  $0.2^\circ$ , the instantaneous torque on the spacecraft is 2.248 Nm, causing a momentum buildup of about 6,000 Nms.

10N bipropellant RCS thrusters selected by the propulsion team will be used to correct for the main thruster misalignment. This correction can be accomplished either by (1) firing the RCS thrusters throughout the burn to counteract the misalignment torque or (2) using the RCS thrusters to spin up the spacecraft to a steady angular rate and thus ‘cancel out’ the torque by varying its direction. A comparison of the momentum (and therefore fuel) costs for both methods was conducted in order to select which method should be used.

---

<sup>75</sup> Larson and Wertz, *Space Mission Analysis and Design*.

<sup>76</sup> Kaela M. Martin and James M. Longuski, “Velocity Pointing Error Reduction for Spinning, Thrusting Spacecraft via Heuristic Thrust Profiles,” *Journal of Spacecraft and Rockets* 52, no. 4 (2015): 1268–1272, accessed May 3, 2022, <https://arc.aiaa.org/doi/10.2514/1.A33152>.

### Constant Corrections Throughout the Burn

Figure 4.3-4 shows the total control momenta, total control torque, and pointing angle deviation for constantly correcting against a misalignment torque of 2.248 Nm over the course of the longest burn time, 90 minutes. Note that the simulation models constant, instantaneous corrections to the misalignment torque that in reality would be accomplished with many impulsive thrusts of the chemical RCS throughout the burn. The total momentum cost from the simulation is  $1.3 \times 10^4$  Nms. The actual momentum cost over the entire transfer is higher than this because there is one longer impulsive burn that lasts for 90 minutes and two shorter impulsive burns that last for 60 minutes. With all three burns combined, the total momentum cost is  $3.34 \times 10^4$  Nms. The required control torques stay at or below 1.5 Nm, which can reliably be executed by the system of 10N chemical RCS. Furthermore, the error on the Euler angles from the desired orientation stays below 0.5°.

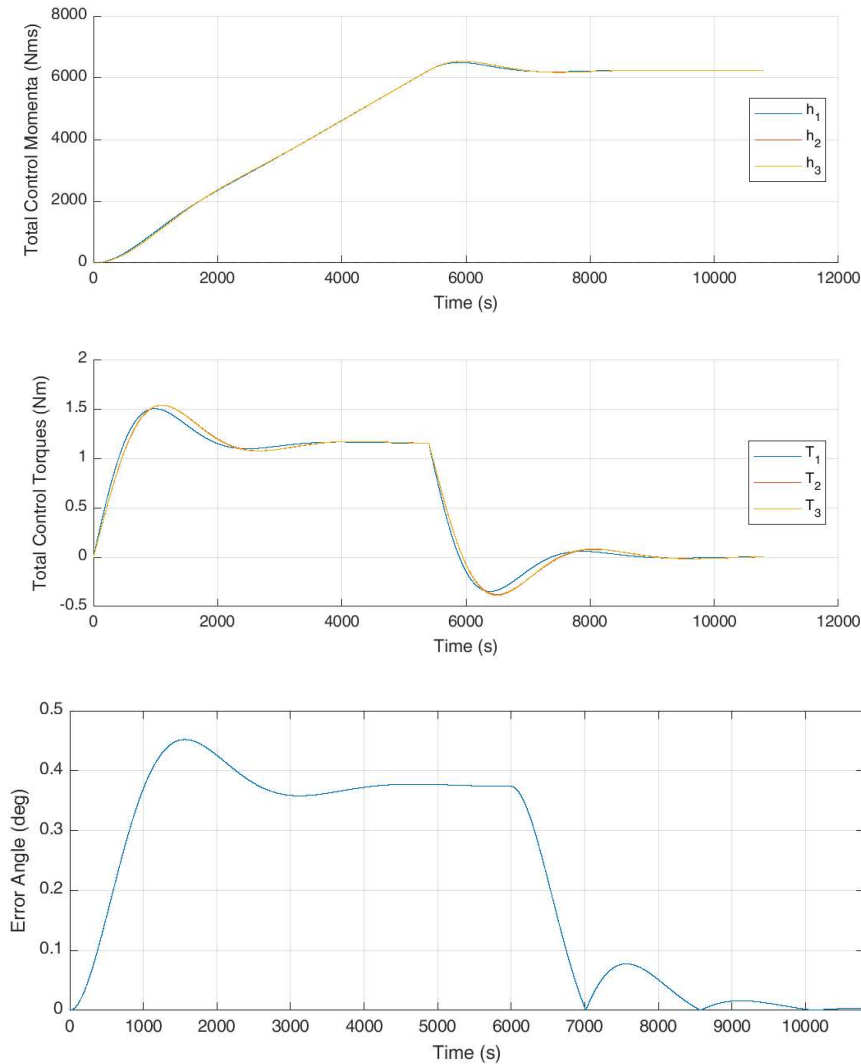


Figure 4.3-4: Thruster Misalignment Simulation for 30-minute Burn (Control Momenta and Torque, Magnitude of Pointing Error During Maneuver).  $k_p = 5e2$ ,  $k_d = 1e5$

### ***Roll Maneuver***

For the second method, also called a roll maneuver, RCS thrusters are used to spin up the spacecraft to a steady angular rate and thus ‘cancel out’ the torque by varying its direction. Since the angular rotation will occur about the  $b_x$  axis (see Figure 4.3-1), the momentum cost for this maneuver can be calculated with Euler’s rotational equations of motion:

$$I_{11} \dot{\omega}_1 = I_{11} \frac{\Delta\omega}{\Delta t} = L_1$$

*Equation 4.3-9*

where  $I_{11}$  is the principle moment of inertia along the  $b_x$  axis,  $\Delta\omega$  is the target angular rate, and  $\Delta t$  is the amount of time needed to accelerate to that angular rate with a constant torque  $L_1$ . For  $I_{11} = 8.13 \times 10^6 \text{ kg m}^2$  (the worst case principle moment for L3), an estimated control torque of 40 Nm, and  $\omega = 0.005 \text{ rad/s}$ ,  $\Delta t = 1016$  seconds, and thus the momentum cost for the RCS thrusters is  $4.07 \times 10^5 \text{ Nms}$ . The actual momentum cost is six times this ( $2.44 \times 10^6 \text{ Nms}$ ) because the same cost would be incurred to spin-down the spacecraft after the duration of the burn, and there are three total impulsive burns. The Euler angle deviation from spinning the spacecraft up to 0.005 rad/s and applying a constant disturbance torque of 2.248 Nm is shown in Figure 4.3-5. A higher angular rate could have been chosen to further decrease the Euler angle deviation, but the total momentum cost for spinning up to 0.005 rad/s is already higher than the momentum cost for constantly correcting throughout the burn. Therefore, the first method of counteracting the misalignment torque with small thrusts over the course of the burn was selected.

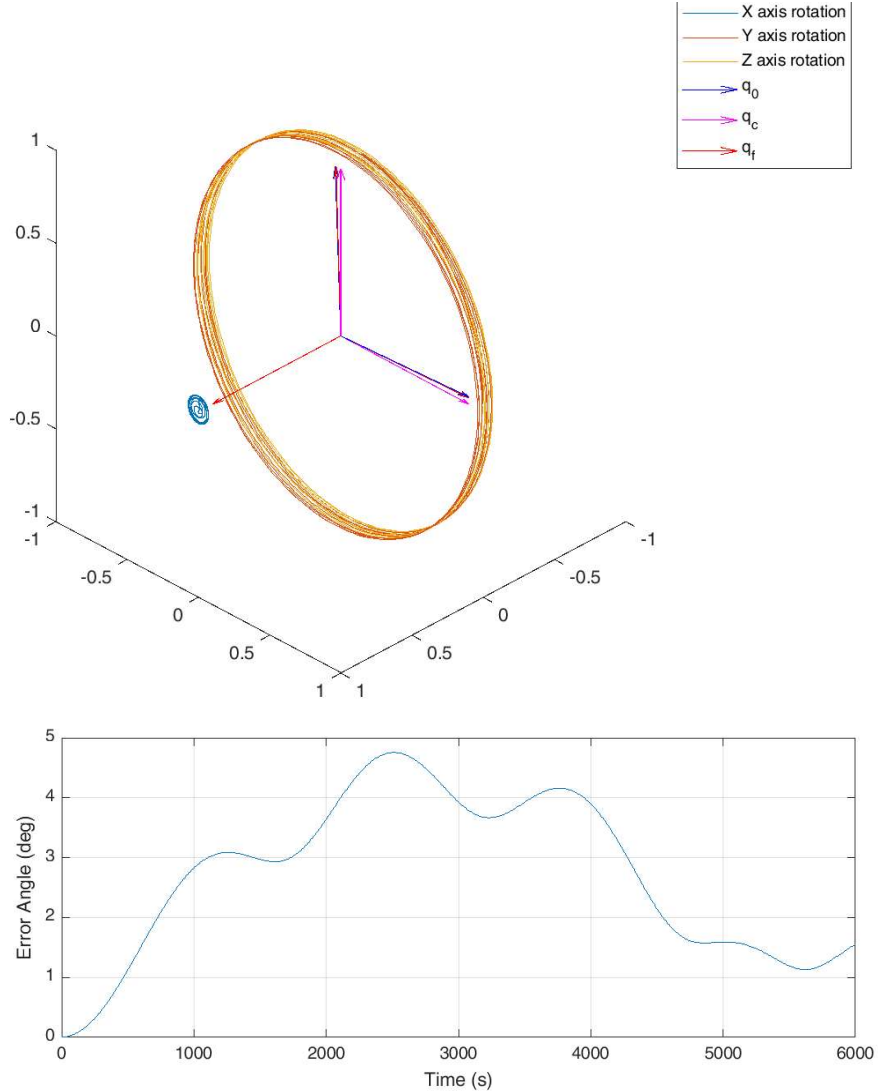


*Figure 4.3-5: Roll Maneuver Simulation with  $\omega = 0.005 \text{ rad/s}$  (Control Momenta and Torque, Orientation of Satellite Body Frame, Magnitude of Pointing Error During Maneuver).*

$$k_p = 1, k_d = 1e4$$

#### 4.3.4.3 Slew Maneuvers

Several slew maneuvers for the L3 and L5 satellites will be required during the transfer from heliocentric orbit to the Lagrange points in order to meet spacecraft thermal needs (see Section 6.3.5.3). There are two  $10^\circ$  and two  $30^\circ$  rotations needed for the L3 satellite. For the L5 satellite, two  $15^\circ$  and two  $30^\circ$  rotations are needed. In addition, it was determined that rotation capabilities up to  $180^\circ$  would be included in the analysis for all three satellites to account for any scenario where an unexpected slew might be required (e.g., worst case scenario after ejection from the launch vehicle or after injection into the halo orbit).

For all of the rotations, it was determined that using RCS thrusters rather than reaction wheels would be necessary to execute the slew because the spacecraft principal moments are large enough such that a reasonable reaction wheel torque would impose a very large power

requirement during transfer mode. The following equation for reaction wheel slew torque from SMAD was used to arrive at this conclusion:

$$T = 4\theta I/t^2$$

Equation 4.3-10

where  $T$  is the required reaction wheel slew torque,  $\theta$  is the rotation angle,  $I$  is the principal moment of the axis of rotation (on the order of  $10^6$ - $10^7$  kg m $^2$  for all three satellites) and  $t$  is the amount of time needed to complete the slew. Based on this equation, a reaction wheel torque of 1.31 Nm would be necessary to complete the slew in one hour. A reaction wheel with this torque capability would require 656-1313 W of power since reaction wheels require 500-1000W of power per Nm of torque.<sup>77</sup> This would double (or triple, for L5) the amount of power needed in transfer mode according to the power budget in Table 5.2-1. Furthermore, 4729 Nms of momentum to accumulate over the 60 minutes, which, for a reaction wheel with a very large 100 Nms momentum storage capacity, would require 47 momentum dumping maneuvers. For these reasons, chemical RCS thrusters were selected as the actuators to perform slew maneuvers.

Slews will be completed by firing the RCS thrusters impulsively to ‘spin-up’ the spacecraft to an angular rate, allowing the spacecraft to rotate at that rate until the desired angular rotation has been achieved, then firing the RCS thrusters in the opposite direction to stop the rotation. A simulation of a 180° rotation, shown in Figure 4.3-6, is performed by inputting only the control input  $q_c$  that represents a 180° rotation from the identity quaternion. The same simulation for a 30° rotation is shown in Figure 4.3-7.

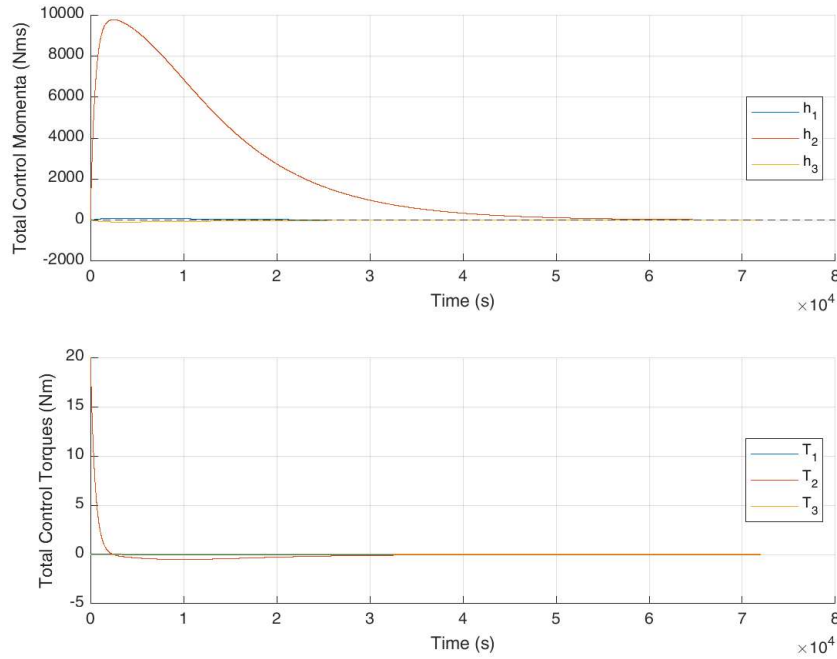
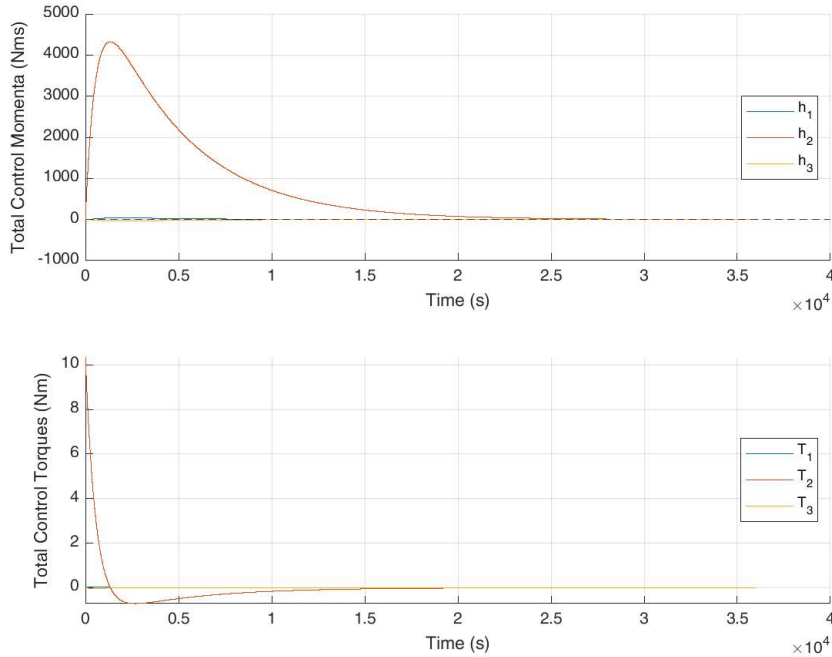


Figure 4.3-6: 180° Rotation Maneuver Simulation (Control Momenta and Torque)

$$k_p = 20, k_d = 1e5$$

---

<sup>77</sup> Larson and Wertz, *Space Mission Analysis and Design*.



*Figure 4.3-7: 30° Rotation Maneuver Simulation (Control Momenta and Torque)*

$$k_p = 40, k_d = 1e5$$

While the net momentum cost of this maneuver would be zero if it were possible to do with reaction wheels alone, there is a nonzero momentum cost associated with using RCS thrusters. Here, the maximum rate of increase of control momenta used (or torque about the spacecraft center of mass) is 20 Nm for a 180° rotation and 10 Nm for a 30° rotation. The plot represents a steep torque with a short duration at the beginning of the maneuver in order to accelerate the satellite, however the majority of the simulation is simply waiting for the rotation to complete. The thermal team did not impose any requirements on the slew rate for these maneuvers, so it was assumed that a relatively long timescale on the order of 8 hours for the 10°, 15°, and 30° rotations and 20 hours for the 180° rotation would be sufficient. This is done in the interest of fuel cost, and in general, the longer the satellite is allowed to perform this maneuver, the lower the fuel cost would be. In practice, this is done simply by adjusting the control gains  $k_p$  and  $k_d$  to increase or decrease the time scale of the step response. Additionally, while the reaction thrusters are modeled as providing a smooth torque in this simulation, in reality they would provide thrust only in short bursts, leading to a slightly longer overall slew time.

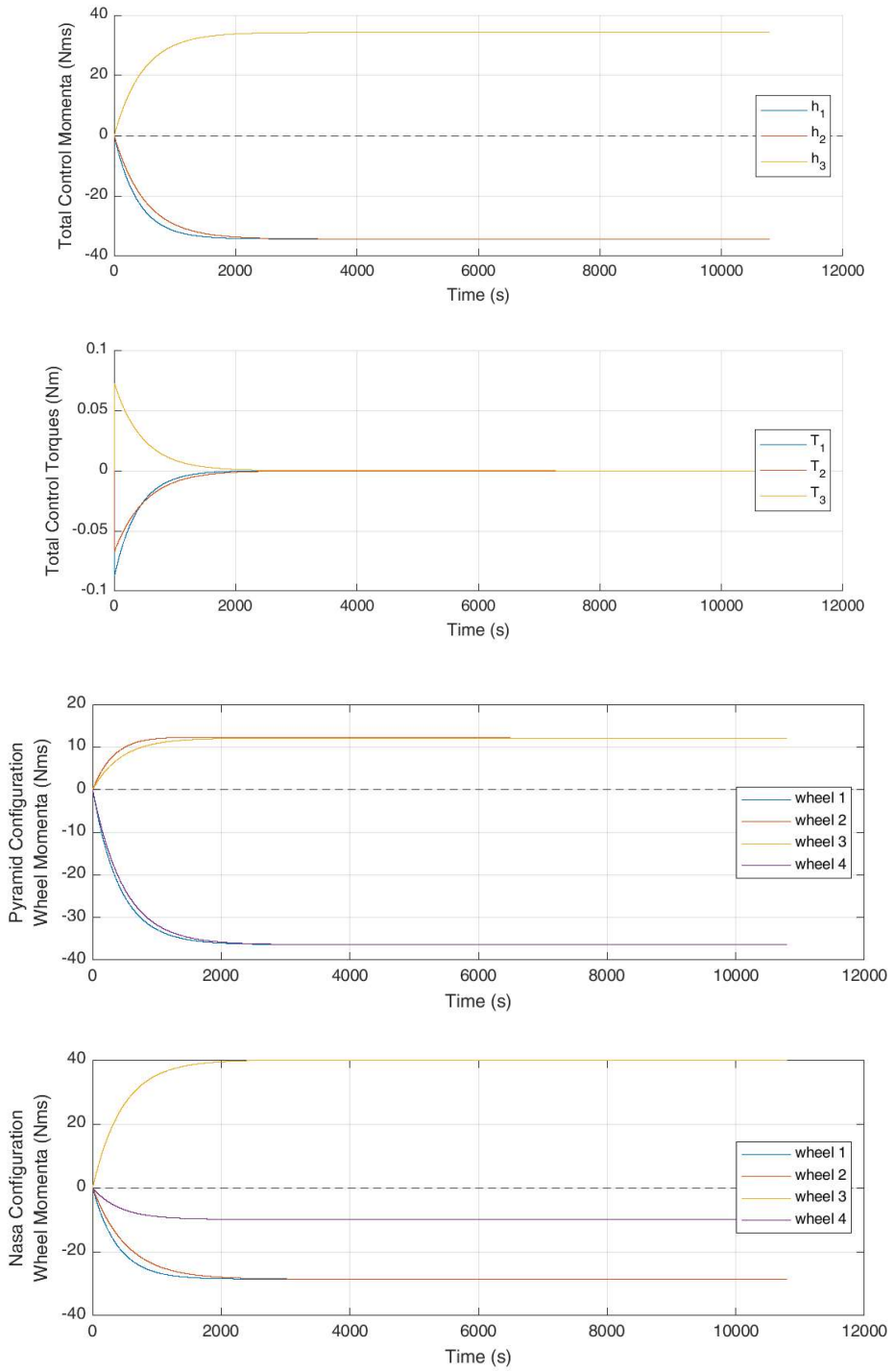
The total momentum costs for all maneuvers over the entire mission lifetime was calculated and passed on to the propulsion team to determine the amount of additional fuel required for ADCS maneuvers.

*Table 4.3-3: Summary of Chemical RCS Momentum Costs for L3*

<b>Maneuver</b>	<b>Number of Maneuvers</b>	<b>Total Momentum Cost (Nms)</b>
Disturbance Rejection	15	$1.147 \times 10^3$
Thruster Misalignment (Long burn)	1	$1.32 \times 10^4$
Thruster Misalignment (Short burn)	2	$1.01 \times 10^4$
10° Slew	2	$1.72 \times 10^4$
30° Slew	2	$1.72 \times 10^4$
Total	-	$5.96 \times 10^4$

#### 4.3.4.4 Detumble Maneuvers (Thruster Misfire)

A key feature of an attitude control system for a satellite is the ability to simply bring all rotations to a stop ( $\dot{q}_c = I_q \ddot{q}$ ), for example, when the satellite is initially detached from the launch vehicle, or if an RCS thruster misfires. In the following simulation, the torque from a single 10 N chemical RCS thruster is inflicted on the satellite as a constant torque not aligned with the principal inertia axes for 10 seconds of burn time. Figure 4.3-4 shows the control momenta and torque along the spacecraft body axes for detumbling the spacecraft in this maneuver.



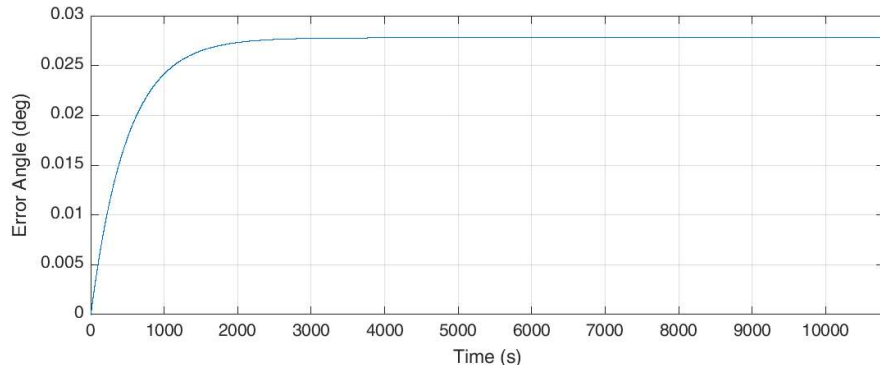


Figure 4.3-8: Detumble Maneuver Control Simulation (Control Momenta and Torque, Control Momenta for Pyramid and NASA configurations, Magnitude of Pointing Error)

$$k_p = 0, k_d = 1e5$$

While instantaneous slews are momentum-free for the most part, detumble maneuvers, such as this one which compensates for an external torque, as well as any maneuver that reduces the initial satellite rotation rate, will result in a net momentum cost incurred. In this simulation (Figure 4.3-8), the momentum cost can be observed by the nonzero steady-state magnitude of 100.685 Nms in the plot of the total control momenta, and in fact that number can be seen as the total momentum cost for this maneuver. From there, decomposing the momentum cost to each wheel in both pyramid and NASA configurations shows that the net momentum cost to the pyramid configuration for this maneuver is 164.463 Nms, and 137.539 Nms for the NASA configuration. In either configuration, the maximum momentum cost to any individual wheel does not exceed 50 Nms, which is well within the maximum capacity of 75 Nms for each individual wheel.

#### 4.3.4.5 Pointing Requirements

##### *Transfer/Acquisition Mode*

The 10° pointing requirement for the Transfer/Acquisition Mode is based on solar array pointing requirements for the NASA Psyche mission during modified low power modes.<sup>78</sup> This ensures the solar arrays can still draw power efficiently (the cosine losses at 10° are small) while also reducing power demands for the ADCS subsystem, since sun sensors can be used in place of star trackers, and there are fewer fine pointing adjustments to be made with reaction wheels.

##### *On-station and Limited Operations Modes*

Based on the revised halo orbits determined by the astrodynamics team, the altitude of the halo orbit (distance from the Lagrange point) is small enough relative to the distance from the Sun to the Lagrange points (at least 1 AU), such that the angle of the spacecraft to the Sun center of mass will always be less than 0.2°, as long as external disturbances and station-keeping are accounted for as described in previous sections. This means that no additional attitude adjustments in the plane of the halo orbit will be required to maintain the 0.2° pointing accuracy.

<sup>78</sup> Lai, Peter. et. al.,. (2021). *Solar Array Pointing Requirements Development for the Psyche Spacecraft*. NASA Jet Propulsion Laboratory.  
<https://trs.jpl.nasa.gov/bitstream/handle/2014/53208/CL%2320-3070.pdf?sequence=1&isAllowed=y>

Thus for all modes where pointing requirements need to be met (transfer, on-station, and limited operation), the only attitude correction driven by pointing requirements is to rotate a small number of degrees per day to keep up with the orbit around the Sun. For the L3, L4, and L5 transfer ellipses, the rates of rotation are  $0.794^\circ/\text{day}$ ,  $0.543^\circ/\text{day}$ , and  $0.444^\circ/\text{day}$ , respectively; these values are calculated with the transfer times and optimized trajectories determined by the orbits team. In on-station mode, the rate of rotation is  $0.986^\circ/\text{day}$  to keep up with the Earth's orbit around the Sun. As the reaction wheels are sized to deal with attitude maneuvers of much larger magnitude, these maneuvers are not the driving requirement for the selection of ADCS hardware.

#### 4.3.5 Hardware Selection and Analysis

##### 4.3.5.1 Sensors

In deciding on a final sensor configuration, three key decisions were made:

1. *Number of Star Trackers*

Because the mission objectives cannot be met if the pointing requirements are not satisfied, it was decided that despite the additional mass, volume, power, and cost considerations, including an additional star tracker for redundancy would be best in order to ensure the greatest chance of mission success.

2. *Coarse vs. Fine Sun Sensors*

Although coarse sun sensors have extremely low mass and no power draw, fine sun sensors were chosen for the mission because they still have relatively low mass and power draw with considerably higher accuracy. Two fine sun sensors are included for redundancy.

3. *Number of Inertial Measurement Units (IMUs)*

Incorporating another IMU would have further increased the overall redundancy of the system, however considering the IMUs secondary role in attitude determination (providing smoothing between star tracker measurements), it was decided that cost in additional mass and volume from an extra IMU did not outweigh the benefit of increased redundancy.

##### ***Star Trackers:***

All of the star trackers considered had a radiation hardness of at least 100 krad and a lifetime of at least 18 years in a GEO orbit. The three primary options considered were the Leonardo A-STR, the Sodern Hydra-TC, and the Spacemicro μSTAR-250. Although the Spacemicro μSTAR-250 has much lower volume, mass, and power budgets, no information could be found on past missions that had flown this instrument. Between the Leonardo A-STR and the Sodern Hydra-TC, the Sodern Hydra-TC was ultimately chosen because of its modular design allowing for the use of two separate optical heads and only 1 fully internally redundant electronic unit, which made it more competitive in terms of mass, volume, and power. In addition, while both the Leonardo and Sodern star trackers have a strong flight heritage on scientific and interplanetary missions, Sodern also has a history of providing custom solutions based on the Hydra line but with additional radiation hardening (specifically for the Europa Clipper mission). This would be an useful option to have in the event that further analysis on the radiation environments at L3, L4, and/or L5 demonstrated the need for additional hardening of components. The full trade study can be found in Table B-3 (1) in Appendix B-3.

### ***Sun Sensor Trade Study:***

The main sun sensors considered for the mission were the Bradford Fine Sun Sensor, the Adcole Digital Sun Sensor, and the S3 Smart Sun Sensor. All of the sun sensors considered had a radiation hardness of at least 100 krad and a lifetime of at least 18 years in GEO. The S3 Smart Sun Sensor was ultimately chosen because of its superior accuracy which will allow for pointing requirements to be met even in low power modes. In addition, it was chosen for the ESA Lisa Pathfinder mission which orbited Sun-Earth L1 point, demonstrating its ability to operate in similar conditions to that which our spacecraft will be encountering. A full trade study can be found in Table B-3 (2) in Appendix B-3.

### ***IMU Trade Study:***

While the Airbus Astrix 200 and L3 Harris Cirrus have superior accuracy and convincing flight heritage, the Honeywell Miniature Inertial Measurement Unit was chosen for its low mass and volume, as well as its proven success on DSCOVR, a scientific mission currently in orbit around the Sun-Earth L1 point. A full trade study can be found in Table B-3 (3) in the Appendix B-3.

#### **4.3.5.2 Actuators**

##### ***RCS Thrusters***

RCS thrusters are incorporated into the ADCS subsystem for the purposes of stationkeeping and momentum dumping. The propulsion team selected chemical thrusters for momentum dumping (see Section 6.1.2.2), both during the transfer to the L3, L4, and L5 points (especially during the main thruster burn), as well as during on-station operations during the halo orbit. Momentum dumping requires full 6-axis control authority of the spacecraft, so the configuration of the chemical RCS thrusters consists of triads located at each corner of the spacecraft. On the sun-pointing face of the spacecraft, three of the thrusters are omitted so that the exhaust plume does not risk damaging the scientific instruments, resulting in a total of 21 chemical thrusters. Hall thrusters will be used for stationkeeping, which does not require full control authority. Therefore there are a total of four Hall thrusters and their configuration is based on where they can unobtrusively fit in between other spacecraft components.

The sizing and selection of both types of RCS thrusters was left to the propulsion subteam. For the chemical thrusters, this was based on the main thruster misalignment torque (Section 4.3.4.2) and external disturbance torques (Section 4.3.2.1). The stationkeeping Hall thrusters were selected based off of the stationkeeping requirement determined by the astrodynamics team.

##### ***Reaction Wheels***

The driving requirement for reaction wheel sizing is disturbance rejection, since all of the slews and thruster misalignment corrections will be accomplished with chemical thrusters. In general, choosing reaction wheels with larger torque and momentum storage capacity than required also helps with minimizing jitter from high wheel speeds.<sup>79</sup> Though the Collins Aerospace RSI 68-170/60 has smaller volume, mass, and power requirements than the Honeywell options, the Honeywell HR14-75 was chosen for its larger momentum storage and

---

<sup>79</sup> Larson and Wertz, *Space Mission Analysis and Design*.

maximum torque authority, which would allow for less frequent momentum dumping and faster realization of attitude adjustments. The momentum storage capacity is 75 Nms, which allows for momentum dumping only about once every year; the maximum torque authority is 0.4 Nm, which is well above the peak disturbance torque. This was chosen over the other two Honeywell models because its smaller volume will allow for better placement close to the spacecraft center of mass. A full trade study can be found in Table B-4 (1) in Appendix B-4.

Additionally, the pyramid configuration was chosen because simulations in previous sections showed that this configuration dissipates momentum on the spacecraft more efficiently than the NASA configuration (e.g., rejecting disturbance torques in Section 4.3.4.1). Furthermore, it was also found that the pyramid configuration responds more predictably when torques or spins are applied in other directions, and that it is also capable of providing a more uniform torque around each body frame axis of the satellite. Therefore, for those reasons the team has chosen to use the pyramid configuration.

#### 4.3.6 Resource Budgets

*Table 4.3-4: ADCS Resource Budgets*

Component	Number	Mass (total, in kg)	Typical Power Draw (total, in W)
Reaction Wheels	4	41.6	48
Hall Thrusters	4	3.92	360
Chemical Thrusters	21	13.65	negligible
Star Tracker	2	6.7	8
Fine Sun Sensor	2	0.660	1
IMU	1	4.7	25
<b>Total</b>	-	<b>71.23</b>	<b>442</b>

Note that there is a discrepancy here with the main mass budget because the chemical and Hall thrusters are included as part of the propulsion subsystem.

#### 4.3.7 Qualitative Risk Analysis

The primary risks associated with the ADCS subsystem come from possible hardware failures (eg. misfired thruster, reaction wheel or star tracker failure) or internal disturbance or noise sources (eg. thruster misalignment, fuel slosh, structural flexibility, and resonance), as shown in Figure 4.3-9. Several risk mitigation strategies have been employed to lower the probability of occurrence and/or severity of these risks. First, possible hardware failures have been incorporated into the overall subsystem design. For example, three reaction wheels are needed for full 3-axis control of the spacecraft, but a fourth has been added for redundancy. There is also a redundant star tracker optical head and sun sensor. Simulations (such as in Section 4.3.4.4 - Detumble) have been performed to ensure that the thrusters and reaction wheels

are capable of handling maneuvers to compensate for hardware failures. In addition, incorporating a Safe Mode ensures that the ADCS subsystem can keep the spacecraft in a halo orbit and meet minimal power and thermal needs in the event of an emergency. The risks associated with fuel slosh, resonance, and structural flexibility will be accounted for in partnership with the structures team by incorporating baffles and rigid appendages. In addition, the elementary control system design is shown to be robust with smooth disturbance rejection to ensure that there are no sudden movements that put the spacecraft structure at risk.

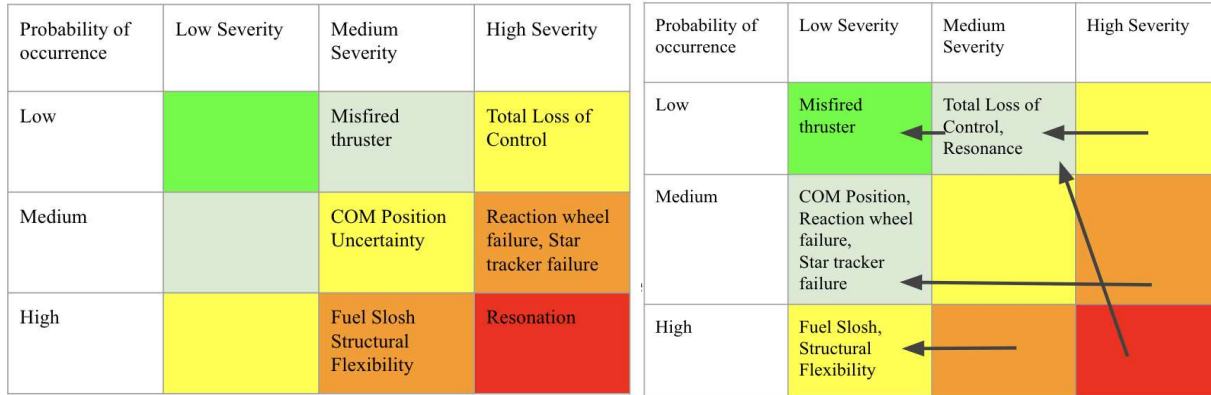


*Figure 4.3-9: ADCS Risk Analysis (left) and Mitigation (right)*

#### 4.3.8 Quantitative Risk Analysis

*Sub-Section Author: Harry Shapiro*

Figure 4.3-8 shows the quantitative fault tree for the ADCS/GNC subsystem. The probabilistic analyses behind this particular tree are explained in-depth in Section 7.1. Probabilistic risk analysis indicates that the most likely components to fail will be RWs and ADCS thrusters, which makes sense given the movement and heat involved, respectively, for those components. However, the redundancy built into the ADCS system ensures that the probability of overall system failure remains low. This analysis was particularly useful for determining the number of thrusters to install and directly drove the decision to install 21 instead of 16 chemical thrusters (which reduced ADCS thrusters' contribution to the 15 year satellite failure probability from 9.61% to 0.02%).

While loss of at least one RW and/or ADCS thruster is virtually inevitable (66.9% at 5 years and 95.2% at 15 years), this does not present an enormous concern due to the significant redundancies built into the ADCS system, which is designed to handle such faults.

Note that Hall thruster failure will not result in complete satellite failure. This is because the chemical thrusters can achieve full 6-axis control authority without the Hall thrusters (albeit somewhat less efficiently). While ADCS and mission life will be degraded if Hall thrusters are lost, the satellite will remain operational.

Likewise, the redundancies built into the GNC system make the probability of total system failure from GNC extremely low.

## Subsystem-Level Fault Tree - ADCS/GNC

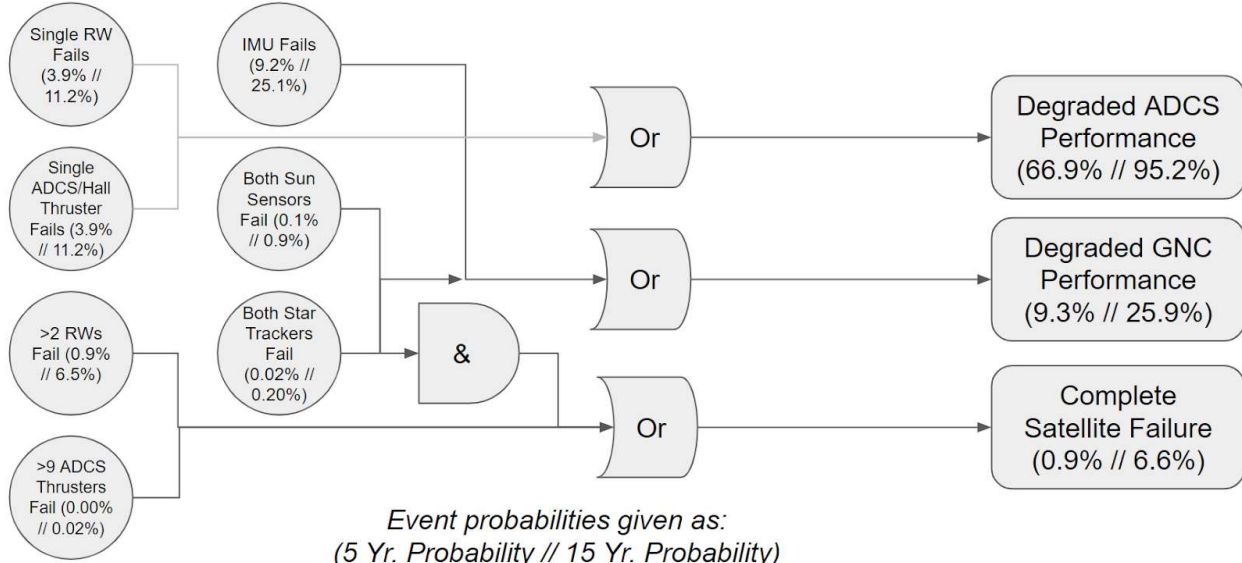


Figure 4.3-10: Fault tree for ADCS/GNC, with associated probabilities. Note that the probabilities given for single RW and thruster failure are the probabilities for each individual RW/thruster, while the “Degraded ADCS Performance” probabilities are for the cumulative probability that at least one RW or thruster fails.